MOX-Report No. 73/2021

A computational study of blood flow dynamics in the pulmonary arteries

Marcinno, F.; Zingaro, A.; Fumagalli, I.; Dede', L.; Vergara, C.

MOX, Dipartimento di Matematica
Politecnico di Milano, Via Bonardi 9 - 20133 Milano (Italy)

mox-dmat@polimi.it http://mox.polimi.it

A computational study of blood flow dynamics in the pulmonary arteries

Fabio Marcinno'[1], Alberto Zingaro[2], Ivan Fumagalli[2], Luca Dede'[2], Christian Vergara[1]

November 28, 2021

[1] LABS, Dipartimento di Chimica, Materiale e Ingegneria Chimica
Politecnico di Milano
fabio.marcinno@mail.polimi.it, christian.vergara@polimi.it

[2] MOX– Modellistica e Calcolo Scientifico
Dipartimento di Matematica
Politecnico di Milano
<alberto.zingaro,ivan.fumagalli,luca.dede>@polimi.it

Keywords: Pulmonary circulation, Hemodynamics, Computational fluid dynamics, Geometric multiscale model, Partitioned coupling algorithm

Abstract

In this work we study for the first time the blood dynamics in the pulmonary arteries by means of a 3D-0D geometric multiscale approach, where a detailed 3D model for the pulmonary arteries is coupled with a lumped parameters (0D) model of the cardiocirculatory system. We propose to investigate two strategies for the numerical solution of the 3D-0D coupled problem: a Splitting Algorithm, where information are exchanged between 3D and 0D models at each time step at the interfaces, and a One-Way Algorithm, where the 0D is solved first off-line. In our numerical experiments performed in a realistic patient-specific 3D domain with a physiologically calibrated 0D model, we discuss first the issue on instabilities that may arise when not suitable connections are considered between 3D and 0D models; second we compare the performance and accuracy of the two proposed numerical strategies. Finally, we report a comparison between an healthy and an hypertensive case, providing a preliminary result highlighting how our method could be used in future for clinical purposes.

1 Introduction

The pulmonary arteries are among the largest arteries in human body, and they are located between the right ventricle and the lungs; they carry de-oxygenated

blood coming from the venous circulation to the pulmonary alveoli, where it is oxygenated [22]. The study of the pulmonary arteries hemodynamics is fundamental since the pulmonary circulation is exposed to critical diseases. One of the most important is Pulmonary Arterial Hypertension (PAH) which leads to an increased resistance to blood flow in the lungs [7, 14].

Computational methods revealed to be an effective, non-invasive tool for the quantitative description of hemodynamics [18,25]. One of the most used computational method in hemodynamics is the *geometric multiscale* approach [26, 29]. In such context, the cardiocirculatory system is divided in two different parts: the part of interest, which is modeled by means of a high detailed model (for example, the 3D Navier-Stokes equations), and the remaining part, which is modeled by means of a geometrically reduced model such as the lumped parameters one, since a detailed description of the hemodynamics outside the region of interest is not needed. We refer to [5, 11, 12, 21, 23, 36] for other works about geometric multiscale coupling.

In this context, the pulmonary circulation is less studied than the systemic arterial one, but in the recent years its interest is increased specially due to the spreading of the Coronavirus COVID19 disease. In [20], the authors simulate the fluid-structure interaction (FSI) of a healthy pulmonary arterial tree using a segregated approach in which the outlet boundary conditions are imposed by means of the Windkessel model; in [19], a FSI of the pulmonary arteries is proposed where traction-free conditions are prescribed at the outlet; in [33], the computational fluid dynamics (CFD) of the pulmonary arteries is simulated under resting and exercise conditions and the outlet boundary conditions are imposed by means of a pure resistance lumped parameter; in [35], the authors simulate FSI in the pulmonary arteries and vary the vessel wall stiffness to simulate different PAH scenarios, with outlet boundary conditions imposed by means of the Windkessel model.

In the present work, we introduce some novelties in the computational hemodynamics of the pulmonary circulation; in particular, we couple the 3D fluid-dynamic model for the pulmonary arteries with a closed-loop lumped parameters model accounting for the whole cardiocirculatory system. This brings to a multiscale 3D-0D problem allowing us to impose physiological outlet conditions to the 3D domain. We consider two different numerical algorithms for the solution of the 3D-0D problem, and the results are compared in terms of hemodynamics variables (velocity, pressure and wall shear stress). Finally, we report a comparison between the healthy and the simulated PAH cases.

The paper outline is as follows. Section 2 is dedicated to the mathematical model of the geometric multiscale coupling. In Section 3 the numerical algorithms are described. Finally, in Section 4 we report the numerical results aiming at showing the reliability of the proposed model, together with a discussion of possible instabilities which may arise in specific conditions.

2 The 3D-0D geometric multiscale model

In medium and large vessels as the pulmonary arteries, blood is well modeled as an incompressible, homogeneus and Newtonian fluid [4,6,25]. Thus, we consider the 3D incompressible Navier-Stokes equations, where $\boldsymbol{u}(\boldsymbol{x},t) : \Omega \times \mathbb{R}^+ \to \mathbb{R}^3$ is the blood velocity, $p(\boldsymbol{x},t) : \Omega \times \mathbb{R}^+ \to \mathbb{R}$ the blood pressure, μ stands for the dynamic blood viscosity, ρ is the blood density and $\boldsymbol{n}$ is the outgoing normal vector from the boundaries. In [20] it has been demonstrated that the rigid wall assumption is able - in first approximation - to well approximate the results obtained by a FSI simulation for the largest branches of the pulmonary arteries since the compliance is not so relevant due to the small pressures. Accordingly, in this work we consider rigid walls. Referring to Figure 1, the 3D computational domain is $\Omega \subset \mathbb{R}^3$, where Γ_{IN} is the inlet boundary, $\Gamma_{OUT,i}$ (with $i = 1, \ldots, 4$) are the outlet boundaries and Γ_W is the vessel wall.

The fluid dynamics of the remaining part of the cardiocirculatory system is modeled by means of a lumped parameters 0D model based on electrical analogies [29]. In particular, the voltage and the current represent the pressure and the blood flow, respectively; the resistance corresponds to the effect of the blood viscosity, the capacity the wall compliance, whereas the inductance the inertial effects of the blood flow. The four cardiac valves are modeled by means of non-ideal diodes, and the heart is described with time dependent elastances representing the pump function [10, 29]. We refer to [31] for the complete list of the differential-algebraic equations of the lumped parameters model. Moreover, we define $\boldsymbol{y}$ as the vector of the state variables and $\boldsymbol{z}$ as the vector of the algebraic variables.

The 3D and 0D models are coupled through suitable interface conditions (I.C.) at the inlet and outlet boundaries guaranteeing the continuity of flow rates and pressures. We refer to the lumped parameter model used here as *Open-0D model*, since it needs to be closed with the 3D model. It is worth noting that the information coming from the 0D model is called *defective* since it prescribes only one scalar function of time over the entire boundary of the 3D domain, thus representing an incomplete information for the 3D formulation [8, 9, 24]. In this work, due to laminar assumption of blood flow that holds true in the pulmonary artery [15, 16], defective flow rate information is completed by means of the prescription of a parabolic velocity profile. Regarding the defective mean pressure condition, a constant and normal pressure is instead prescribed according to the *do-nothing* approach, see [13].

Thus, let us define T as the final time of the simulation, therefore the strong formulation of the geometric multiscale 3D-0D model reads as follows:

find $\boldsymbol{u}$, p and $\boldsymbol{y}, \boldsymbol{z}$, for any $t \in (0, T]$, such that

$$
\begin{cases}
3D \begin{cases}
\rho \dfrac{\partial \boldsymbol{u}}{\partial t} + \rho(\boldsymbol{u} \cdot \nabla)\boldsymbol{u} - \nabla \cdot \boldsymbol{T}(\boldsymbol{u}, p) = \boldsymbol{0} & \text{in} \quad \Omega, \\
\nabla \cdot \boldsymbol{u} = 0 & \text{in} \quad \Omega, \\
\boldsymbol{u}(\boldsymbol{x}, 0) = \boldsymbol{0} & \text{in} \quad \Omega, \\
\boldsymbol{u}(\boldsymbol{x}, t) = \boldsymbol{0} & \text{on} \quad \Gamma_W,
\end{cases} \\
I.C. \begin{cases}
Q_{IN} = \displaystyle\int_{\Gamma_{IN}} \boldsymbol{u} \cdot \boldsymbol{n} \, d\Gamma \,, \\
P_{IN} = \dfrac{1}{|\, \Gamma_{IN} \,|} \displaystyle\int_{\Gamma_{IN}} p \, d\Gamma \,, \\
Q_{OUT} = \displaystyle\int_{\Gamma_{OUT}} \boldsymbol{u} \cdot \boldsymbol{n} \, d\Gamma \,, \\
P_{OUT} = \dfrac{1}{|\, \Gamma_{OUT} \,|} \displaystyle\int_{\Gamma_{OUT}} p \, d\Gamma \,,
\end{cases} \\
Open - 0D \begin{cases}
\dfrac{d}{dt}\boldsymbol{y} = f_1^O(t, \boldsymbol{y}, \boldsymbol{z}, P_{IN}, Q_{OUT}) \,, \\
\boldsymbol{y}(0) = \boldsymbol{y}_0 \,, \\
\boldsymbol{z} = f_2^O(t, \boldsymbol{y}) \,,
\end{cases}
\end{cases}
$$

where $\boldsymbol{T} = -p\,\boldsymbol{I} + \mu\,\nabla\boldsymbol{u}$, $\Gamma_{OUT} = \sum_{i=1}^{4} \Gamma_{OUT,i}$, f_1^O and f_2^O are the right hand side terms of the differential and algebraic equations of the Open-0D model. It is worth reporting the equations describing the heart chambers and the cardiac valves; in particular the elastance E has the following structure:

$$
E(t) = E_a\, r(t) + E_b \,, \quad r(t) = \begin{cases}
\frac{1}{2}\left(1 - \cos\left(\frac{\pi t}{T_{contr}}\right)\right) & t \le T_{contr} \,, \\
\frac{1}{2}\left(1 + \cos\left(\frac{\pi t}{T_{relax}}\right)\right) & t > T_{contr} \,,
\end{cases}
$$

where E_a and E_b are the active and passive elastances, respectively, T_{contr} is the duration of the chamber contraction and T_{relax} is the duration of the chamber relaxation. The resistance of the cardiac valves is in general defined as follows:

$$
\begin{aligned}
R = 10^c \,, \quad c = log_{10}R_{min} + (log_{10}R_{max} - log_{10}R_{min}) \times \\
\times \left[\frac{1}{2} + \frac{1}{\pi}\arctan\left(\frac{200\pi}{2}\,(P_2 - P_1)\right)\right] \,,
\end{aligned}
$$

where R_{max} is the resistance when the valve is closed and R_{min} corresponds to the resistance when the valve is open, and P_1 and P_2 are the pressures upstream and downstream the valve, respectively.

In Figure 1, we report the representation of the geometric multiscale model highlighting the zones of interest (the resistance of the cardiac valves is omitted).

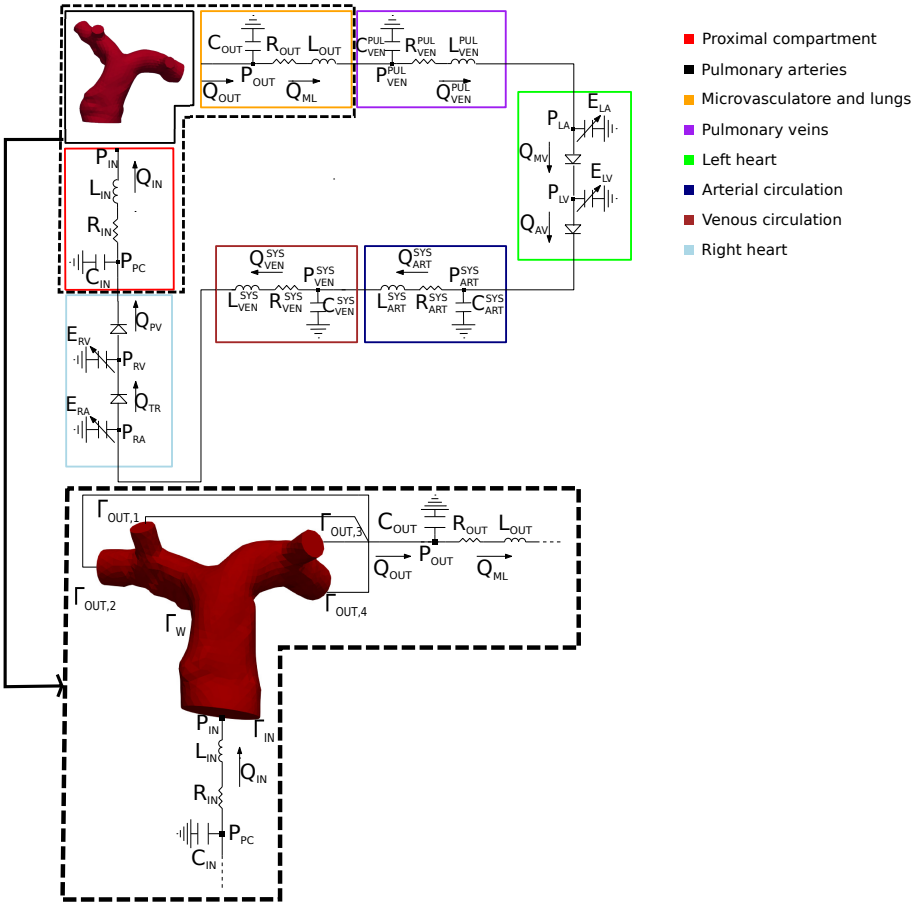

Figure 1: Top: Geometric multiscale model of the entire cardiocirculatory system obtained by the coupling between the 3D pulmonary artery and the Open-0D model. Bottom: Zoom on the region where the 3D-0D coupling occurs. In the squares the four interface variables.

Notice from Figure 1 that we couple the 3D model not directly with the pulmonary valve (diode, light blue block) in the upstream region. Instead, we introduce an additional block, denoted as "proximal compartment" and colored in red in Figure 1, representing the proximal part of the pulmonary artery. We couple the inlet of the 3D model to the proximal compartment, and we found that this coupling choice preserves the appearance of instabilities, as we better discuss in Section 4.2.

3 Algorithms for the numerical solution

In order to numerically solve the geometric multiscale model, we introduce a uniform time discretization in which $\Delta t = \frac{T}{N_t}$ is the step size, and N_t are the number of steps in which the time interval is subdivided. The n-th temporal

time step is defined as $t^n = n\Delta t$ for $n = 0, \dots, N_t$. Given a function of time $v(t)$, we denote by $v^n \simeq v(t^n)$ its approximation after the time discretization.

Concerning the 3D model, the time discretization is obtained by means of the first order backward differentiation formula (implicit Euler) and the convective term is treated with a semi-implicit treatment [28]. The time discretization of the 0D model is achieved by means of the 4^{th} order Runge-Kutta explicit method [27].

For the solution of the coupled geometric multiscale problem, we introduce two strategies: the *Splitting Algorithm* and the *One-Way Algorithm*, described in what follows.

3.1 The Splitting Algorithm

The geometric multiscale coupling is solved through a *partitioned* and *explicit* way; this means that the lumped parameter model and the 3D model are solved sequentially once per time step by means of different numerical solvers through the exchange of information at the interfaces.

The algorithm is constructed as follows: at time t^{n+1} the 3D model receives from the Open-0D model the flow rate datum Q_{IN}^n computed at previous time step imposed at the inlet Γ_{IN} by means of a parabolic velocity profile, i.e. $\boldsymbol{u}^{n+1} = \boldsymbol{g}$, with

$$\int_{\Gamma_{IN}} \boldsymbol{g} \cdot \boldsymbol{n}\, d\Gamma = Q_{IN}^n, \qquad \boldsymbol{g}(r) = -2\frac{Q_{IN}^n}{\pi R^2}\left(1 - r^2/R^2\right)\boldsymbol{n},$$

where R is the radius of the circle located at the inlet of the pulmonary artery and obtained by considering a small flow extension of the reconstructed inlet [1], and r is the radial coordinate. Moreover, it receives the mean pressure datum P_{OUT}^n imposed at each of the four in parallel outlets $\Gamma_{OUT,i}$ by means of the do-nothing approach, i.e

$$\boldsymbol{T}(\boldsymbol{u}^{n+1}, p^{n+1})\boldsymbol{n} = -P_{OUT}^n\,\boldsymbol{n} \qquad \text{on} \quad \Gamma_{OUT,i} \times (0,T] \qquad i = 1, \dots, 4.$$

We use for the 3D fluid dynamics the compact notation $F(\boldsymbol{u}^{n+1}, p^{n+1}) = 0$ together with the interface boundary conditions involving Q_{IN}^n and P_{OUT}^n, which allows to compute the other two interface data P_{IN}^{n+1} and Q_{OUT}^{n+1}. These latter information are passed to the Open-0D model as forcing terms. In particular, we compactly use for the Open-0D model the notation
$\boldsymbol{y}^{n+1} = f_1(t^n; \boldsymbol{y}^n, \boldsymbol{z}^{n+1}, P_{IN}^{n+1}, Q_{OUT}^{n+1})$ and $\boldsymbol{z}^{n+1} = f_2(t^n, \boldsymbol{y}^n))$ which is solved allowing to compute the quantities Q_{IN}^{n+1} and P_{OUT}^{n+1} for the next time step.

We report the Splitting scheme in Algorithm 1.

Algorithm 1 Splitting Algorithm.

while $t^{n+1} \leq T$ **do**

SOLVE the 3D problem:

$F(\boldsymbol{u}^{n+1}, p^{n+1}) = 0,$

$$\int_{\Gamma_{IN}} \boldsymbol{u}^{n+1} \cdot \boldsymbol{n}\, d\Gamma = Q_{IN}^{n} \quad \rightarrow \quad \boldsymbol{u}^{n+1} = \boldsymbol{g}(r) \quad \text{on} \quad \Gamma_{IN}\,,$$

$$\frac{1}{|\,\Gamma_{OUT,i}\,|} \int_{\Gamma_{OUT,i}} \boldsymbol{T}(\boldsymbol{u}^{n+1}, p^{n+1})\boldsymbol{n}\, d\Gamma = -P_{OUT}^{n} \quad \rightarrow$$

$$\rightarrow \quad \boldsymbol{T}(\boldsymbol{u}^{n+1}, p^{n+1})\boldsymbol{n} = -P_{OUT}^{n}\boldsymbol{n} \quad \text{on} \quad \Gamma_{OUT,i};$$

COMPUTE the *interface* data:

$$P_{IN}^{n+1} = \frac{1}{|\,\Gamma_{IN}\,|} \int_{\Gamma_{IN}} p^{n+1}\, d\Gamma\,,$$

$$Q_{OUT}^{n+1} = \int_{\Gamma_{OUT,i}} \boldsymbol{u}^{n+1} \cdot \boldsymbol{n}\, d\Gamma\,;$$

$P_{IN}^{n+1}, Q_{OUT}^{n+1} \rightarrow Open - 0D\,;$

SOLVE the Open-0D model:

$\boldsymbol{z}^{n+1} = f_2^O\left(t^n; \boldsymbol{y}^n\right),$

$\boldsymbol{y}^{n+1} = f_1^O\left(t^n; \boldsymbol{y}^n, \boldsymbol{z}^{n+1}, P_{IN}^{n+1}, Q_{OUT}^{n+1}\right);$

$Q_{IN}^{n+1}, P_{OUT}^{n+1} \rightarrow 3D;$

$n \rightarrow n+1.$

end while

3.2 The One-Way Algorithm

The One-Way algorithm couples the 3D and the *Closed-0D model* obtained by the Open-0D model inserting a RLC circuit representing the pulmonary artery (see the black box in Figure 2).

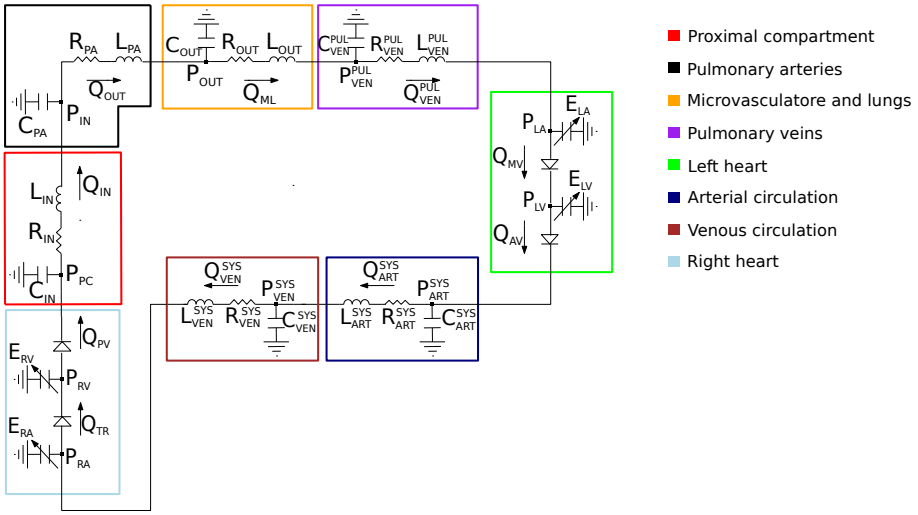

Figure 2: Closed-0D model used in the One-Way Algorithm. Q_{IN} and P_{OUT} are provided to the 3D pulmonary arteries (Algorithm 2). Notice the 3D pulmonary arteries compartment, here is replaced by the black RLC network.

In this case the coupling is only in one direction; in particular, the Closed-0D model is solved off-line independently. Afterward, at each time step t^n the 0D flow rate Q_{IN}^n and the mean pressure P_{OUT}^n are passed to the 3D model, without any feedback to the Closed-0D model.

We report the One-Way scheme in Algorithm 2.

Algorithm 2 One-Way Algorithm.

while $t^{n+1} \leq T$ **do**

SOLVE the Closed-0D model:

$\boldsymbol{z}^{n+1} = f_2^C\left(t^n; \boldsymbol{y}^n\right),$

$\boldsymbol{y}^{n+1} = f_1^C\left(t^n; \boldsymbol{y}^n, \boldsymbol{z}^{n+1}\right);$

end while

while $t^{n+1} \leq T$ **do**

$Q_{IN}^{n+1}, P_{OUT}^{n+1} \rightarrow 3D;$

SOLVE the 3D problem:

$F(\boldsymbol{u}^{n+1}, p^{n+1}) = 0,$

$$\int_{\Gamma_{IN}} \boldsymbol{u}^{n+1} \cdot \boldsymbol{n}\, d\Gamma = Q_{IN}^{n+1} \quad \rightarrow \quad \boldsymbol{u}^{n+1} = \boldsymbol{g}(r) \quad \text{on} \quad \Gamma_{IN}\,,$$

$$\frac{1}{|\,\Gamma_{OUT,i}\,|} \int_{\Gamma_{OUT,i}} \boldsymbol{T}(\boldsymbol{u}^{n+1}, p^{n+1})\boldsymbol{n}\, d\Gamma = -P_{OUT}^{n+1} \quad \rightarrow$$

$$\rightarrow \quad \boldsymbol{T}(\boldsymbol{u}^{n+1}, p^{n+1})\boldsymbol{n} = -P_{OUT}^{n+1}\boldsymbol{n} \quad \text{on} \quad \Gamma_{OUT,i}.$$

end while

where f_1^C and f_2^C are the right hand side terms of the differential and algebraic equations of the Closed-0D model.

3.3 Space discretization

For the solution of the 3D problem in both Algorithms 1 and 2, we consider the Finite Elements approximation. In particular, we use $\mathbb{Q}1$-$\mathbb{Q}1$ Finite Elements for the approximation of the pressure and each velocity component, introducing $X_1^h(\Omega) = \{\boldsymbol{v}_h^{n+1} \in C^0(\Omega) : \boldsymbol{v}_h^{n+1} \in \mathbb{Q}1, \forall K \in T_k\}$, where T_k is a triangulation of hexahedral cells K, together with a stabilization term to ensure uniqueness of the solution given by the PSPG technique. Moreover, to guarantee stability of the numerical solution in presence of a dominated advection regime, we also include the SUPG stabilization [28]. Finally, due to the presence of backflows at the outlets that lead to the production of instabilities due to the lack of energy dissipation of the convective term, we also add a *backflow stabilization* non-consistent term [3].

Thus, the fully discretized formulation reads as follows: for every $n =$

$0, 1, \ldots, N_t - 1$, find $\boldsymbol{u}_h^{n+1} \in \boldsymbol{V}^h$ and $p_h^{n+1} \in Q^h$ such that

$$\left(\rho\left(\frac{\boldsymbol{u}_h^{n+1}-\boldsymbol{u}_h^n}{\Delta t}\right), \boldsymbol{v}_h\right) + \left(\rho\boldsymbol{u}_h^n \cdot \nabla \boldsymbol{u}_h^{n+1}, \boldsymbol{v}_h\right) + \left(\mu\nabla\boldsymbol{u}_h^{n+1}, \nabla\boldsymbol{v}_h\right) - \left(p_h^{n+1}, \nabla\cdot\boldsymbol{v}_h\right) +$$
$$+ \int_{\Gamma_{OUT,i}} \beta\frac{\rho}{2}\left(\boldsymbol{u}_h^n\cdot\boldsymbol{n}\right)_- \boldsymbol{u}_h^{n+1}\cdot\boldsymbol{v}_h\, d\Gamma + s_h(\boldsymbol{u}_h^{n+1}, p_h^{n+1}; \boldsymbol{v}_h, q_h) =$$
$$= \int_{\Gamma_{OUT,i}} P_{OUT}^n \boldsymbol{n}\cdot\boldsymbol{v}_h\, d\Gamma \qquad \forall \boldsymbol{v}_h \in \boldsymbol{W}^h,$$
$$(\nabla\cdot\boldsymbol{u}_h^{n+1}, q_h) = 0, \qquad \forall q_h \in Q^h,$$
$$\boldsymbol{u}_h^0 = \boldsymbol{0} \qquad \text{in } \Omega\,,$$

where $\boldsymbol{V}^h = \{\boldsymbol{v} \in [X_1^h(\Omega)]^3 : \boldsymbol{v}_{\Gamma_{IN}} = \boldsymbol{g},\, \boldsymbol{v}_{\Gamma_W} = \boldsymbol{0}\}$, $Q^h = X_1^h(\Omega)$, $\boldsymbol{W}^h = \{\boldsymbol{v} \in [X_1^h(\Omega)]^3 : \boldsymbol{v}_{\Gamma_{IN}\cup\Gamma_w} = \boldsymbol{0}\}$, β is the backflow stabilization parameter, and s_h is the SUPG-PSPG stabilization term [34].

4 Numerical results

In this section, we present some numerical results of the proposed computational models to handle the geometric multiscale coupling in the pulmonary arteries. First, we report the results of mesh convergence (Sect. 4.2). Second, we discuss the presence of possible numerical instabilities and how to stabilize the solution (Sect. 4.3). Then, we report the results obtained with the two proposed numerical algorithms and we analyze their differences in terms of velocity, pressure and wall shear stresses (WSS) (Sect. 4.4). In Sect. 4.5 we discuss the accuracy of the Closed-0D model in comparison with the 3D-0D one. Finally, in Sect. 4.6 we report a comparison between a healthy and a Pulmonary Arterial Hypertension (PAH) cases.

4.1 Numerical experiments setting

The numerical algorithms were implemented in life^{x}[1], a high-performance object-oriented Finite Element library focused on the mathematical models and numerical methods for cardiac applications. It is developed in the iHEART[2] project at the MOX Laboratory, Dipartimento di Matematica, Politecnico di Milano. The numerical simulations were run on clusters with processor Xeon E5-2640 v4 with 20 core, a base frequency of 20 GHz, and with RAM of 63 GB.

The 3D computational domain of the pulmonary arteries is reconstructed from CT scans provided by the Division of Cardiovascular Surgery of "Luigi Sacco" Hospital, Milan, by means of the Vascular Modeling ToolKit (VMTK, see

[1] https://lifex.gitlab.io/

[2] iHEART - An Integrated Heart model for the simulation of the cardiac function. European Research Council (ERC) grant agreement No 740132.

[2]), which allows also to generate the corresponding hexahedral computational mesh (see Sect. 4.2).

We set the blood density $\rho = 1.06 \cdot 10^3 \, \frac{\text{Kg}}{\text{m}^3}$, dynamic viscosity $\mu = 3.5 \cdot 10^3 \, \text{Pa} \cdot \text{s}$, time step $\Delta t = 0.001 \, \text{s}$ and a heartbeat period $T = 0.8 \, \text{s}$. The linear system arising after linearization and discretization is solved by means of the GMRES method with a maximum number of iterations equal to 1000 and an absolute tolerance of 10^{-10}. The backflow stabilization (see Sect. 3.3) is applied on every outlet boundary with $\beta = 1$.

In Table 1, we report all the values of the lumped parameters used in the 0D models of the two algorithms. Notice that common values used in the Open- and Closed-0D models were taken from [36]. Instead, the specific values (in caps in the table) used in the black box of the Closed-0D model representing the pulmonary artery were calibrated in order to maximize the accordance between the 3D-0D and the Closed-0D results.

4.2 Test I: Mesh convergence

We carry out a mesh convergence study to investigate the accuracy of our numerical solution by refining the grid. To this aim, we consider here three grids having a different space step discretization, namely:

- Fine grid, $h_1 = 2.22 \, \text{mm}$,
- Medium grid, $h_2 = 3.50 \, \text{mm}$,
- Coarse grid, $h_3 = 5.50 \, \text{mm}$.

It is worth noting that the space discretization steps have a constant ratio, $r = \frac{h_2}{h_1} = \frac{h_3}{h_2} = 1.6$. On a longitudinal slice, obtained by cutting the 3D pulmonary artery, we compute the integrals f_i, $i = 1, 2, 3$, of the pressure field for the three grids, used as *indices* for the convergence analysis. Then, we estimate the order of convergence (p), the constant of the numerical method (c) and the reference solution (f_{ref}), by means of the Richardson extrapolation [32],

$$p = \frac{log(\frac{f_3 - f_2}{f_2 - f_1})}{log(r)}, \quad f_{ref} = \frac{(h_2^p \cdot f_3 - h_3^p \cdot f_2)}{(-h_3^p + h_2^p)}, \quad c = (f_3 - f_{ref})/h_3^p .$$

Finally, we compute the relative discrepancies among the meshes as follows:

$$E_i = \frac{\mid f_i - f_{ref} \mid}{\mid f_{ref} \mid}, \qquad i = 1, 2, 3.$$

Given the value of r used in this analysis, an acceptable value for the relative discrepancy under which we can argue that the solution has reached convergence, is 3%.

Table 1: Resistance ($\frac{mmHg \cdot s}{ml}$), inductance ($\frac{mmHg \cdot s^2}{ml}$), capacity ($\frac{ml}{mmHg}$) and elastance ($\frac{mmHg}{ml}$) values of both (Open- and Closed-) 0D models. In caps the values of the pulmonary artery block, holding only for the Closed-0D model.

Right atrium	E_a	0.06
	E_b	0.07
	T_{contr}	0.17
	T_{relax}	0.17
Tricuspid valve	R_{min}	$75{\cdot}10^{-3}$
	R_{max}	$75{\cdot}10^{3}$
Right ventricle	E_a	0.55
	E_b	0.05
	T_{contr}	0.34
	T_{relax}	0.15
Pulmonary valve	R_{min}	$75{\cdot}10^{-3}$
	R_{max}	$75{\cdot}10^{3}$
Proximal compartment	R_{IN}	$3.21{\cdot}10^{-2}$
	L_{IN}	$2.50{\cdot}10^{-3}$
	C_{IN}	3.90
PULMONARY ARTERY	R_{PA}	$2.50{\cdot}10^{-4}$
	L_{PA}	$2{\cdot}10^{-3}$
	C_{PA}	$5{\cdot}10^{-4}$
Microvasculature and lungs	R_{OUT}	$2.29{\cdot}10^{-2}$
	L_{OUT}	$1.65{\cdot}10^{-3}$
	C_{OUT}	0.25
Pulmonary venous system	R_{VEN}^{PUL}	$3.56 \cdot 10^{-2}$
	L_{VEN}^{PUL}	$5{\cdot}10^{-4}$
	C_{VEN}^{PUL}	16
Left atrium	E_a	0.07
	E_b	0.09
	T_{contr}	0.17
	T_{relax}	0.17
Mitralic valve	R_{min}	$75{\cdot}10^{-3}$
	R_{max}	$75{\cdot}10^{3}$
Left ventricle	E_a	2.75
	E_b	0.08
	T_{contr}	0.34
	T_{relax}	0.15
Aortic valve	R_{min}	$75{\cdot}10^{-3}$
	R_{max}	$75{\cdot}10^{3}$
Systemic arterial system	R_{ART}^{SYS}	0.64
	L_{ART}^{SYS}	$5{\cdot}10^{-3}$
	C_{ART}^{SYS}	1.2
Systemic venous system	R_{VEN}^{SYS}	0.26
	L_{VEN}^{SYS}	$5{\cdot}10^{-4}$
	C_{VEN}^{SYS}	60

Table 2: For the three different meshes: Total number of grid cells N, index f_i used for the convergence analysis, relative discrepancy E_i. Mesh convergence. Test I.

Mesh	N	f_i	$E_i(\%)$
Coarse	26692	6.754	4.9
Medium	84992	6.774	2.9
Fine	298176	6.785	1.8

In Table 2, we report the quantitative values used to perform the mesh convergence. From these results, we find that the mesh with an average cell size $h = 3.5\,\text{mm}$, corresponding to 84992 cells (see Figure 3), satisfies the convergence requirement, namely, a relative error less than 3%. Thus, we decide to use it for the all the numerical simulations.

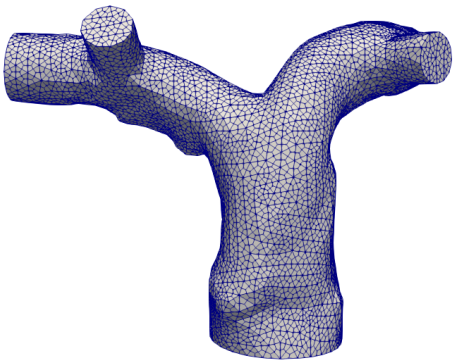

Figure 3: Hexahedral mesh of the patient-specific pulmonary artery used for all the numerical tests, anterior view. Test I.

It is worth noting that the simulations for the grid convergence were done with a fixed time step of $10^{-3}\,\text{s}$ that guaranteed that the temporal error was below the spatial one.

4.3 Test II: About the stability of coupling algorithms

In Section 2 we have discussed the introduction of a RLC model (the red one in Figure 1) between the 3D pulmonary artery and the pulmonary valve (downstream diode in the light blue block). This RLC model represents the first $0.3\,cm$ of the pulmonary artery and allows to avoid the direct connection of the 3D model with the diode, which, as detailed below for the first time, may lead to unstable results. This lumped parameter model must be suitably devised to guarantee a correct mathematical transition between the models.

In order to valuate the effect of this RLC model on the Splitting and One-

Way algorithms, we considered first a scenario where in the Open-0D model, such block is eliminated and the 3D model is connected directly with the pulmonary valve diode (light blue block). We refer to this scenario as Setting 1, see Figure 4, left.

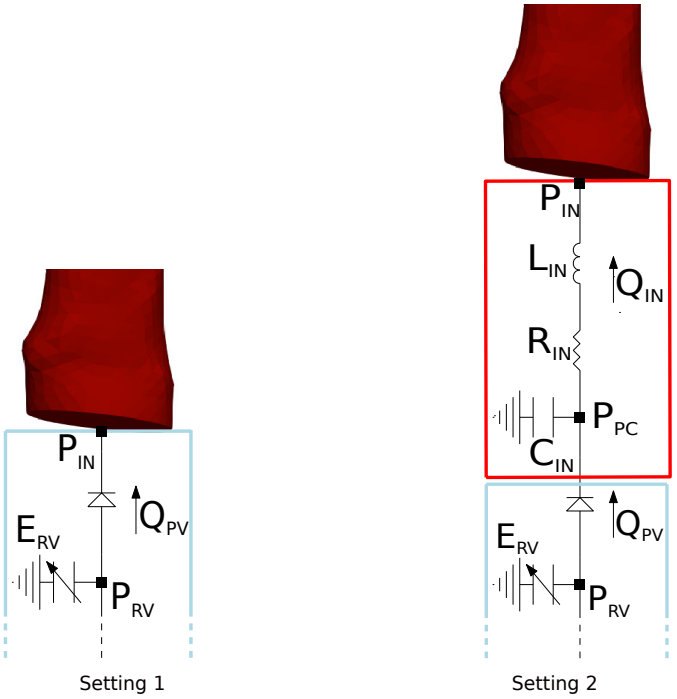

Figure 4: Left: The 3D model is directly connected with the pulmonary valve (Setting 1). Right: The 3D model is connected with the complete Open-0D models (Setting 2). Test II.

In Figure 5 we report for the Splitting Algorithm the inlet quantities together with the ventricular pressure computed by the 0D model. Similar results are obtained for the One-Way Algorithm. In particular, the inlet flow rate Q_{IN} is computed by the 0D model whereas the inlet mean pressure P_{IN} by the 3D model. We can observe unstable solutions just after the first time steps in the case of Setting 1. The arising of such instabilities seems to be independent of the choice of the time step Δt. Moreover, varying the resistance of the non-ideal diode modeling the pulmonary valve does not introduce any improvement. Instead, the complete Open-0D model accounting also for the RLC (red block) lumped model (Setting 2, see Figure 4, right), allows to get stable results.

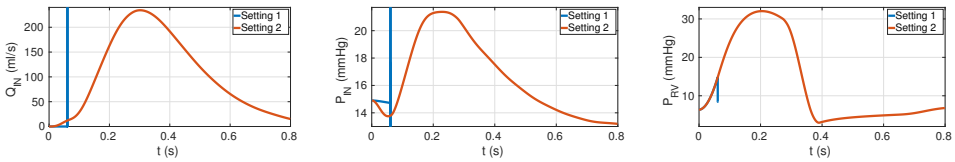

Figure 5: Comparison between the results obtained with Setting 1 (blue) and Setting 2 (red). Left: 0D inlet flow rate (Q_{IN}). Right: 3D inlet mean pressure (P_{IN}). Bottom: 0D right ventricular pressure (P_{RV}). Test II.

The previous behaviours could be explained by observing that in Splitting Algorithm for 3D-0D coupling the concept of *bridging regions* plays a fundamental role [29]. In particular, when the 3D model gives to the Open-0D model an information about the pressure, the latter becomes a forcing term for the Open-0D model making necessary the presence of an inductive term at the interface to allow the calculation of the flow rate representing a state variable for the Open-0D model. On the other hand, if the 3D model gives an information about the flow rate to the Open-0D model, a compliance must be present at the interface, in order to calculate the pressure representing a state variable for the Open-0D model. Thus, the direct connection of the 3D model with the diode does not guarantee, for both Splitting and One-Way Algorithms, the satisfaction of such principle and this explains the unstable solutions.

Notice also that the results obtained with the complete Open-0D model (Setting 2) are in good agreement with the physiological ranges [30, 35].

4.4 Test III: Comparison between coupling algorithms

In this section, we report and discuss the results obtained by means of the two coupling algorithms introduced in Section 3, namely the Splitting Algorithm and the One-Way Algorithm. In particular, in Figure 6 we report for a longitudinal slice the comparison between velocity fields at three different temporal instants of the heartbeat, namely the acceleration phase ($t = 1.75\,\mathrm{s}$), the systolic peak ($t = 1.9\,\mathrm{s}$) and the deceleration phase ($t = 2.15\,\mathrm{s}$). The results do not present any relevant difference in terms of flow pattern and magnitude. We observe a recirculation region in the inferior side of the right pulmonary artery during the systolic peak. Some vortices are generated during the deceleration phase, which are slightly different in the two cases.

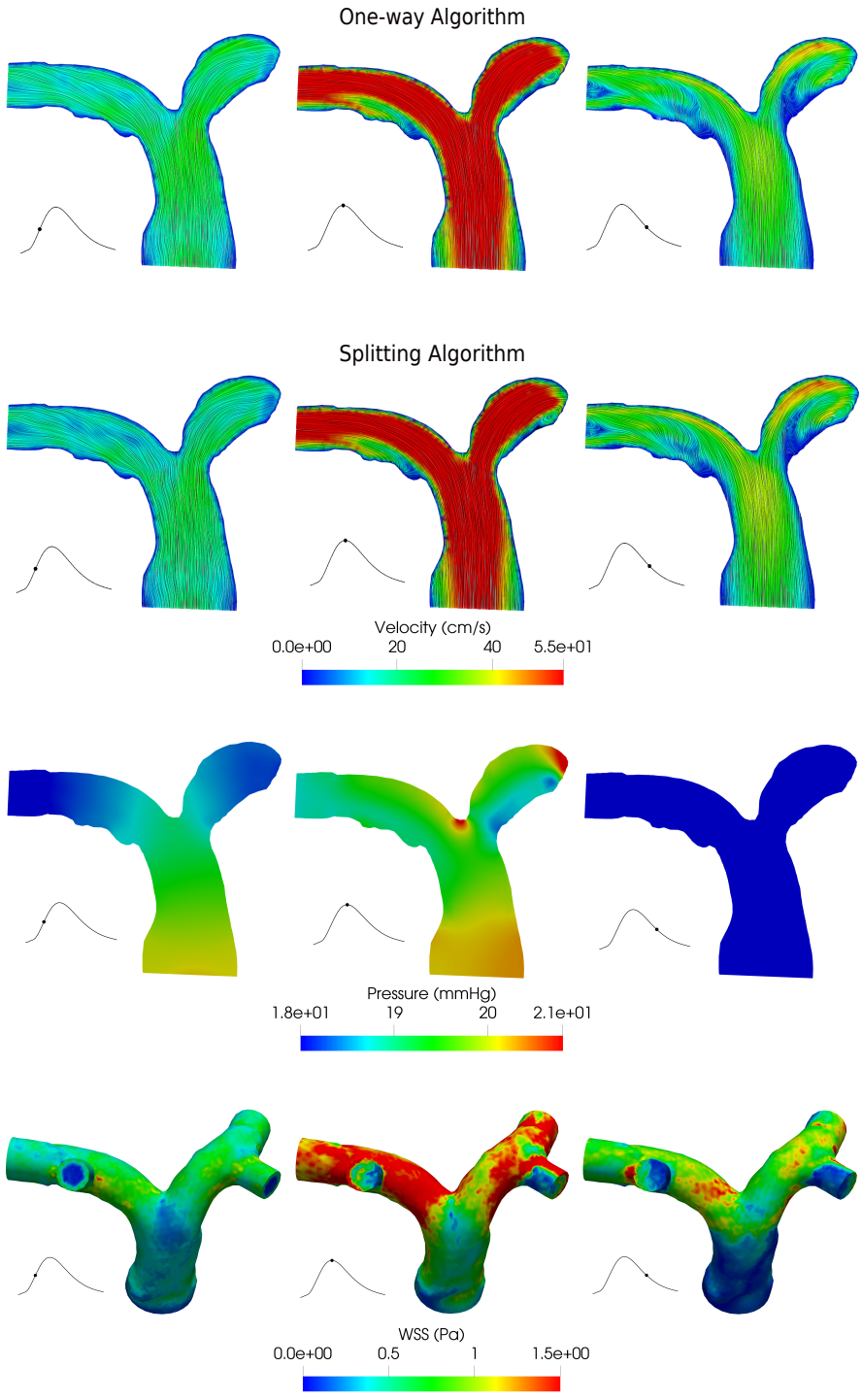

Figure 6: Left: Acceleration phase ($t = 1.75\,\mathrm{s}$). Center: Systolic peak ($t = 1.9\,\mathrm{s}$). Right: Deceleration phase ($t = 2.15\,\mathrm{s}$). Test III.

On the same section, we also report the pressure field obtained with the Splitting Algorithm. The solution of the One-Way Algorithm is almost identical, thus it is not shown. At the systolic peak, a high pressure is experienced at the inlet. On the branching of the left and right pulmonary arteries, there is a stagnation point that generates the highest pressure of the whole pulmonary arteries.

Finally, in the same figure, we show the WSS field on the physical wall, again only for the Splitting algorithm since relevant differences are not found between the two algorithms. WSS measures the tangential viscous stress exerted by the blood in motion onto the vessel walls [10]:

$$WSS = \|\boldsymbol{T}\,\boldsymbol{n} - (\boldsymbol{T}\boldsymbol{n}\,\boldsymbol{n})\boldsymbol{n}\|\,,$$

where $\boldsymbol{T}$ represents the Cauchy stress tensor. In particular, the WSS is reported from the anterior view in order to highlight the differences between the main and distal branches. The WSS magnitude is strongly related to the velocity, therefore we see an higher WSS in the distal branches of the pulmonary vasculature where the diameter of the vessel decreases.

The results obtained with this test show that the proposed method is able to simulate the hemodynamics of the pulmonary arteries obtaining physiological results in accordance with [20].

We finally observe that both the algorithms require comparable computational time of about 24 hours to simulate five heartbeats.

4.5 Test IV: About the accuracy of the Closed-0D model

The Closed-0D model (i.e the model where the 3D pulmonary artery is substituted with a 0D model, black box in Figure 2) allows the calculation of the mean pressure and flow rate in the whole cardio-circulatory system with a convenient computational cost; therefore, it is a powerful framework that can give a quantitative indication about the haemodynamics at least in terms of averaged flow properties as mean pressures and flow rates. In Figure 7, we compare the mean pressure and the flow rate inside the pulmonary artery compartment computed by the Closed-0D model with those computed by means of the 3D model for both the Splitting and One-Way Algorithms.

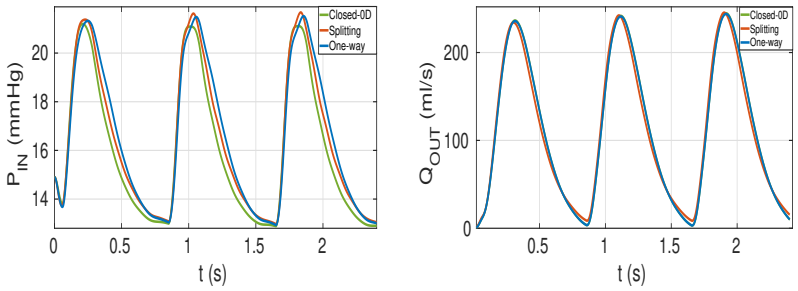

Figure 7: Interface quantites. Left: Inlet pressure (P_{IN}). Right: Outlet flow rate (Q_{OUT}). Test IV.

From these results, we notice that the Closed-0D model, properly calibrated (see Table 1), is able to give accurate results able to capture almost perfectly the mean quantities, i.e the inlet mean pressure and the outlet flow rate. In the flow rate, we are not able to see any difference, instead in the pressure field, the models present the bigger differences at the systolic peak and during the deceleration phase. Of course, to have a fully detailed description of the blood flow, as the local pressure, velocity field and WSS, a 3D-0D coupled model is needed (see Figure 1).

4.6 Test V: Comparison between healthy and Pulmonary Arterial Hypertension cases

In this final test, we compare the hemodynamics in the pulmonary artery in the healthy and PAH diseases. To this aim, we use the Splitting Algorithm. The PAH is a disease characterized by an elevated resistance in the distal branches of the pulmonary arteries (the microvasculature and the lungs compartment); this condition entails an increase in the working pressure of the right ventricle, possibly causing hypertrophy and failure [17]. It has been demonstrated that the hemodynamics parameters are significant indicators of PAH; in particular, changes in the right ventricle end-diastolic volume and a decrease of WSS at the proximal part of the pulmonary artery are suggested as a good indicator of PAH severity [35]. We model the PAH disease by increasing the resistance of microvascolature and lungs compartment: specifically, we quintuplicate the R_{OUT} value with respect to the physiological case choosing $R_{OUT} = 1.14 \cdot 10^{-1} \, \frac{\text{mmHg} \cdot \text{s}}{\text{ml}}$.

Using the same visualizations of Figure 1, in Figure 8 we compare the velocity, pressure and WSS fields of the healthy and simulated PAH cases at the systolic peak ($t = 1.9\,\text{s}$).

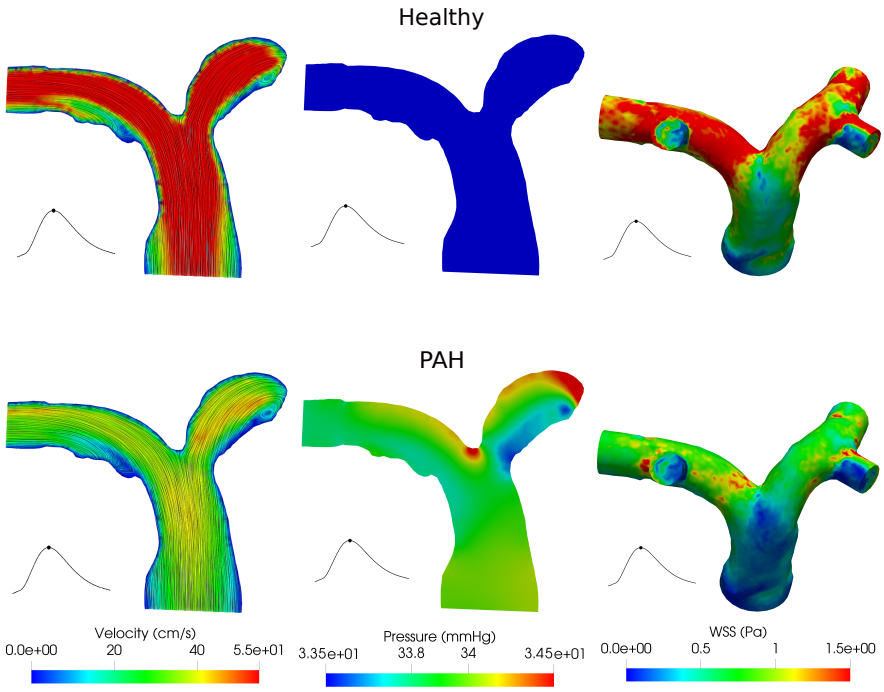

Figure 8: Systolic peak ($t = 1.9\,\mathrm{s}$). Left: Velocity field. Center: Pressure field. Right: WSS field. Test V.

From these results, we observe that the PAH is characterized by a strong decrease in term of velocity due to the resistance increase of the 0D microvasculature and lungs compartment representing physically the distal branches of the pulmonary arteries. This increase leads to a higher pressure along the whole pulmonary artery, and consequently to lower velocities. Since the WSS is strongly related with the velocity field, we find that the PAH is also associated with a lower WSS than the healthy case, specially in the distal branches. It is worth noting that in the PAH disease, the pressure reached at the systolic peak is about 34 mmHg, almost 1.5 times more than the pressure reached in the healthy case.

5 Conclusions and Limitations

We have simulated the hemodynamics of the pulmonary arteries in a geometric multiscale context. Physiological inlet and outlet boundary conditions are provided to the 3D model of the pulmonary arteries by means of a lumped parameter model of the entire cardiocirculatory system.

We adopted two strategies for the coupling of the 3D and 0D models: the One-Way and the Splitting Algorithms. In the first one, the models are coupled only in one direction, without any feedback from the 3D to the 0D model. In the second one, the 3D and the Open-0D models are fully coupled with an explicit (in time) strategy. Numerical results have demonstrated that both the algorithms

are able to reproduce physiological results in accordance with the literature. The two algorithms provide substantially equivalent results in terms of velocity and WSS, and some slight differences for the pressure.

We have also simulated PAH disease increasing the resistance of the microvasculature and lungs compartment. We found that, as expected, PAH produces a strong increase of the pressures with respect to the healthy case and consequently, lower velocites and WSS, in particular in the distal branches.

This study presents some limitations. First, the 3D pulmonary arteries were modeled by means of the rigid walls assumption. This is a restrictive choice because it leads to an overestimation of pressure, velocity and WSS, especially in the distal branches, as found in [20]; for a simulation including the 3D model of the microvasculature, the fluid-structure interaction approach becomes mandatory. Moreover, the pulmonary arterial stiffness seems to be one of the principal biomechanical markers for the identification of PAH disease [35], therefore an FSI simulation may give more accurate information about PAH.

Second, the lumped parameter model of the cardiocirculatory system is relatively simple; other RLC compartments could be added in order to consider different parts of the cardiocirculatory system.

To conclude, at the best of our knowledge, this work is the first attempt to insert the 3D pulmonary artery in a geometric multiscale context, therefore, it can be seen as the foundation for a future FSI simulation of the pulmonary artery using a geometric multiscale approach.

References

[1] Luca Antiga, Marina Piccinelli, Lorenzo Botti, Bogdan Ene-Iordache, Andrea Remuzzi, and David A Steinman. An image-based modeling framework for patient-specific computational hemodynamics. *Medical & biological engineering & computing*, 46(11):1097–1112, 2008.

[2] Luca Antiga, Marina Piccinelli, Lorenzo Botti, Bogdan Ene-Iordache, Andrea Remuzzi, and David A Steinman. An image-based modeling framework for patient-specific computational hemodynamics. *Medical & biological engineering & computing*, 46(11):1097–1112, 2008.

[3] Y Bazilevs, JR Gohean, TJR Hughes, RD Moser, and Y25718211229 Zhang. Patient-specific isogeometric fluid–structure interaction analysis of thoracic aortic blood flow due to implantation of the jarvik 2000 left ventricular assist device. *Computer Methods in Applied Mechanics and Engineering*, 198(45-46):3534–3550, 2009.

[4] Nikolay Bessonov, Adélia Sequeira, Sergey Simakov, Yu Vassilevskii, and Vitaly Volpert. Methods of blood flow modelling. *Mathematical modelling of natural phenomena*, 11(1):1–25, 2016.

[5] P.J. Blanco, S.A. Urquiza, and R.A. Feijòo. Assessing the influence of heart rate in local hemodynamics through coupled 3d-1d-0d models. *Int J Num Meth Biomed Eng*, 26:890–903, 2010.

[6] S. Canic. Fluid-structure interaction in blood flow. pages 11–15. MSRI Publication Series, 2007.

[7] D Chemla, Vincent Castelain, P Herve, Y Lecarpentier, and Serge Brimioulle. Haemodynamic evaluation of pulmonary hypertension. *European Respiratory Journal*, 20(5):1314–1331, 2002.

[8] L. Formaggia, J.F. Gerbeau, F. Nobile, and A. Quarteroni. Numerical treatment of defective boundary conditions for the Navier-Stokes equation. *SIAM J Num An*, 40(1):376–401, 2002.

[9] L. Formaggia, A. Veneziani, and C. Vergara. Flow rate boundary problems for an incompressible fluid in deformable domains: formulations and solution methods. *Comp Meth Appl Mech Eng*, 199 (9-12):677–688, 2009.

[10] Luca Formaggia, Alfio Quarteroni, and Alessandro Veneziani. *Cardiovascular Mathematics: Modeling and simulation of the circulatory system*, volume 1. 2010.

[11] Luca Formaggia, Alfio Quarteroni, and Christian Vergara. On the physical consistency between three-dimensional and one-dimensional models in haemodynamics. *Journal of Computational Physics*, 244:97–112, 2013.

[12] Luca Formaggia and Alessandro Veneziani. Geometrical multiscale models for the cardiovascular system. In *Blood flow modelling and diagnostic*, volume 6, pages 309–359. Institute of Fundamental Technological Research of the Polish Academy of Science, 2005.

[13] John G Heywood, Rolf Rannacher, and Stefan Turek. Artificial boundaries and flux and pressure conditions for the incompressible Navier–Stokes equations. *International Journal for numerical methods in fluids*, 22(5):325–352, 1996.

[14] Marius M Hoeper, Hossein-Ardeschir Ghofrani, Ekkehard Grünig, Hans Klose, Horst Olschewski, and Stephan Rosenkranz. Pulmonary hypertension. *Deutsches Ärzteblatt International*, 114(5):73, 2017.

[15] Keith Horsfield and Michael J Woldenberg. Diameters and cross-sectional areas of branches in the human pulmonary arterial tree. *The Anatomical Record*, 223(3):245–251, 1989.

[16] Liwei Hu, Rongzhen Ouyang, Aimin Sun, Qian Wang, Chen Guo, Yafeng Peng, Yan Qin, Yong Zhang, Yang Xiang, and Yumin Zhong. Pulmonary artery hemodynamic assessment of blood flow characteristics in repaired

tetralogy of fallot patients versus healthy child volunteers. *Quantitative Imaging in Medicine and Surgery*, 10(5):921, 2020.

[17] VO Kheyfets, W O'Dell, T Smith, JJ Reilly, and EA Finol. Considerations for numerical modeling of the pulmonary circulation - A review with a focus on pulmonary hypertension. *Journal of Biomechanical engineering*, 135(6):061011, 2013.

[18] Hyun Jin Kim, Irene E Vignon-Clementel, C Alberto Figueroa, John F LaDisa, Kenneth E Jansen, Jeffrey A Feinstein, and Charles A Taylor. On coupling a lumped parameter heart model and a three-dimensional finite element aorta model. *Annals of biomedical engineering*, 37(11):2153–2169, 2009.

[19] Fande Kong, Vitaly Kheyfets, Ender Finol, and Xiao-Chuan Cai. Simulation of unsteady blood flows in a patient-specific compliant pulmonary artery with a highly parallel monolithically coupled fluid-structure interaction algorithm. *International journal for numerical methods in biomedical engineering*, 35(7):e3208, 2019.

[20] Ju Liu, Weiguang Yang, Ingrid S Lan, and Alison L Marsden. Fluid-structure interaction modeling of blood flow in the pulmonary arteries using the unified continuum and variational multiscale formulation. *Mechanics Research Communications*, 107:103556, 2020.

[21] A.C.I. Malossi, P.J. Blanco, S. Deparis, and A. Quarteroni. Algorithms for the partitioned solution of weakly coupled fluid models for cardiovascular flows. *Int J Num Meth Biomed Eng*, 27:2035—-2057, 2011.

[22] Elaine N. Marieb. *Essentials of Anatomy and Physiology*. 4 edition, 2008.

[23] Mahdi Esmaily Moghadam, Irene E Vignon-Clementel, Richard Figliola, Alison L Marsden, Modeling of Congenital Hearts Alliance (MOCHA) Investigators, et al. A modular numerical method for implicit 0d/3d coupling in cardiovascular finite element simulations. *Journal of Computational Physics*, 244:63–79, 2013.

[24] A. Porpora, P. Zunino, C. Vergara, and M. Piccinelli. Numerical treatment of boundary conditions to replace lateral branches in haemodynamics. *Int. J. Numer. Meth. Biomed. Eng.*, 28(12):1165–1183, 2012.

[25] A. Quarteroni, L. Dede', A. Manzoni, and C. Vergara. Mathematical modelling of the human cardiovascular system - Data, numerical approximation, clinical applications. *Cambridge University Press*, 2019.

[26] Alfio Quarteroni, Stefania Ragni, and Alessandro Veneziani. Coupling between lumped and distributed models for blood flow problems. *Computing and Visualization in Science*, 4(2):111–124, 2001.

[27] Alfio Quarteroni, Fausto Saleri, and Paola Gervasio. *Calcolo scientifico*. 2008.

[28] Alfio Quarteroni and Alberto Valli. *Numerical approximation of partial differential equations*, volume 23. 2008.

[29] Alfio Quarteroni, Alessandro Veneziani, and Christian Vergara. Geometric multiscale modeling of the cardiovascular system, between theory and practice. *Computer Methods in Applied Mechanics and Engineering*, 302:193–252, 2016.

[30] Parameter Equation Normal Range. Normal hemodynamic parameters–adult. *Peter R. Lichtenthal, MD*, page 105, 2002.

[31] Francesco Regazzoni, Matteo Salvador, Pasquale Claudio Africa, Marco Fedele, Luca Dede, and Alfio Quarteroni. A cardiac electromechanics model coupled with a lumped parameters model for closed-loop blood circulation. part i: model derivation. *arXiv preprint arXiv:2011.15051*, 2020.

[32] Patrick J Roache. Quantification of uncertainty in computational fluid dynamics. *Annual review of fluid Mechanics*, 29(1):123–160, 1997.

[33] Beverly T Tang, Tim A Fonte, Frandics P Chan, Philip S Tsao, Jeffrey A Feinstein, and Charles A Taylor. Three-dimensional hemodynamics in the human pulmonary arteries under resting and exercise conditions. *Annals of biomedical engineering*, 39(1):347–358, 2011.

[34] Tayfun Tezduyar and Sunil Sathe. Stabilization parameters in SUPG and PSPG formulations. *Journal of computational and applied mechanics*, 4(1):71–88, 2003.

[35] Byron A Zambrano, Nathan McLean, Xiaodan Zhao, Ju-Le Tan, Liam Zhong, C Alberto Figueroa, Lik Chuan Lee, and Seungik Baek. Patient-specific computational analysis of hemodynamics and wall mechanics and their interactions in pulmonary arterial hypertension. *Frontiers in bioengineering and biotechnology*, 8:1536, 2020.

[36] Alberto Zingaro, Ivan Fumagalli, Luca Dede, Marco Fedele, Pasquale Claudio Africa, Antonio Francesco Corno, and Alfio Quarteroni. A multiscale cfd model of blood flow in the human left heart coupled with a lumped-parameter model of the cardiovascular system. *arXiv preprint arXiv:2110.02114*, 2021.

MOX Technical Reports, last issues

Dipartimento di Matematica
Politecnico di Milano, Via Bonardi 9 - 20133 Milano (Italy)

70/2021 Beirao da Veiga, L.; Canuto, C.; Nochetto, R.H.; Vacca, G.; Verani, M.
Adaptive VEM: Stabilization-Free A Posteriori Error Analysis

71/2021 Franco, N.; Manzoni, A.; Zunino, P.
A Deep Learning approach to Reduced Order Modelling of parameter dependent Partial Differential Equations

72/2021 Fresca, S.; Manzoni, A.
POD-DL-ROM: enhancing deep learning-based reduced order models for nonlinear parametrized PDEs by proper orthogonal decomposition

69/2021 Antonietti, P.F.; Caldana, M.; Dede', L.
Accelerating Algebraic Multigrid Methods via Artificial Neural Networks

65/2021 Mazzieri, I.; Muhr, M.; Stupazzini, M.; Wohlmuth, B.
Elasto-acoustic modelling and simulation for the seismic response of structures: The case of the Tahtali dam in the 2020 Izmir earthquake

66/2021 Antonietti, P.F.; Botti, M.; Mazzieri, I.
On mathematical and numerical modelling of multiphysics wave propagation with polygonal Discontinuous Galerkin methods

67/2021 Salvador, M.; Regazzoni, F.; Pagani, S.; Dede', L.; Trayanova, N.; Quarteroni, A.
The role of mechano-electric feedbacks and hemodynamic coupling in scar-related ventricular tachycardia

68/2021 Regazzoni, F.; Salvador, M.; Dede', L.; Quarteroni, A.
A machine learning method for real-time numerical simulations of cardiac electromechanics

63/2021 Rosafalco, L.; Torzoni, M.; Manzoni, A.; Mariani, S.; Corigliano, A.
Online structural health monitoring by model order reduction and deep learning algorithms

64/2021 Clarotto, L; Allard, D.; Menafoglio, A.
A new class of alpha-transformations for the spatial analysis of Compositional Data